Zhou *et al.*
Progress in Earth and Planetary Science (2023) 10:59
https://doi.org/10.1186/s40645-023-00591-x

Progress in Earth and Planetary Science

RESEARCH ARTICLE

Open Access

Interannual variation of the Warm Arctic–Cold Eurasia pattern modulated by Ural blocking and the North Atlantic Oscillation under changing sea ice conditions

Xiling Zhou[1*], Tomonori Sato[2] and Shixue Li[1]

Abstract

Together with rapid Arctic warming and sea ice decline, especially over the Barents–Kara seas (BKS), extreme cold winters have occurred frequently in mid-latitudes, particularly in Central Eurasia. A pattern with two distinct winter temperature anomalies centered over the BKS and Central Eurasia is known as the Warm Arctic–Cold Eurasia (WACE) pattern. The impacts of sea ice loss over the BKS and internal atmospheric variability on past WACE formation remain under discussion mainly due to the large internal atmospheric variability in the mid-latitudes. This study analyzed a large-ensemble historical experiment prescribing observed sea ice condition to investigate the role of internal atmospheric variability in the observed interannual variation of the WACE pattern. Comparison of ensemble members suggests that internal atmospheric variability is important for regulating the magnitude of the WACE pattern. Besides the strong effect of local sea ice loss, winter temperature over the BKS increases due to warm advection driven by the Ural blocking and positive phase of the North Atlantic Oscillation. A decrease in winter temperature over Central Eurasia is mainly attributable to the cold advection enhanced by Ural blocking rather than the remote effect of sea ice decline over the BKS. Our study reveals the importance of internal atmospheric variability in elucidating the observed interannual variation of the WACE pattern.

Keywords Warm Arctic–Cold Eurasia pattern, Sea ice loss, Ural blocking, North Atlantic Oscillation

1 Introduction

Synchronous with rapid Arctic warming, the sea ice area has declined dramatically over the Arctic Ocean, especially over the Barents–Kara seas (BKS) since the 1990s (Stroeve and Notz 2018; Isaksen et al. 2022; Rantanen et al. 2022), enhancing turbulent heat flux from the surface to the atmosphere (Kim et al. 2019). Nevertheless, extreme cold winters with increased freezing days and decreased minimum temperatures have occurred frequently in mid-latitudes, especially in Central Eurasia (CEU) (Cohen et al. 2014; McCusker et al. 2016; Johnson et al. 2018). This pattern with two distinct winter temperature anomalies centered over the BKS and CEU is known as the Warm Arctic–Cold Eurasia (WACE) pattern, which is characterized as the second leading mode of winter surface air temperature (SAT) over Eurasia (Mori et al. 2014). Despite the dedicated research effort in recent years on the causes of both the frequent cold winters in Eurasia and the WACE pattern, the mechanism linking the Arctic and the mid-latitude winter climate remains to be fully elucidated (e.g., Inoue et al. 2012; McCusker et al. 2016; Sun et al. 2016; Zhang et al.

*Correspondence:
Xiling Zhou
zhouxiling@ees.hokudai.ac.jp
[1] Graduate School of Environmental Science, Hokkaido University, N10W5, Sapporo, Hokkaido 060-0810, Japan
[2] Faculty of Environmental Earth Science, Hokkaido University, N10W5, Sapporo, Hokkaido 060-0810, Japan

2018; Blackport et al. 2019; He et al. 2020; Wang and Chen 2022).

It has been proposed that sea ice decline over the BKS has influenced the recent cold winters in Eurasia (e.g., Inoue et al. 2012; Mori et al. 2019), and that modulation of cyclone tracks and the troposphere-stratosphere pathway is responsible for the remote effect of sea ice loss (Inoue et al. 2012; Kim et al. 2014; Nakamura et al. 2015; Zhang et al. 2018). Inoue et al. (2012) suggested that lower baroclinicity over the Barents Sea in low ice conditions reduces the eastward progression of cyclones, which leads to an anticyclonic anomaly over the Siberian coast that causes anomalous warm advection over the Barents Sea and cold advection over eastern Siberia. Zhang et al. (2018) pointed out that the downward influence of the stratospheric circulation anomaly, in response to late autumn sea ice loss, intensifies the ridge near the Ural Mountains and the trough over East Asia, favoring cold winters in Siberia. Nakamura et al. (2015) proposed that recent sea ice reduction in late autumn is linked to the negative phase of the Arctic Oscillation/North Atlantic Oscillation (NAO) in winter, resulting in cold advection toward mid-latitudes.

Some studies have suggested that sea ice decline is not a crucial factor for cold winters in Eurasia (e.g., McCusker et al. 2016; Blackport et al. 2019; Blackport and Screen 2021), and that the formation of the WACE pattern is mainly attributable to internal atmospheric variability (e.g., Li et al. 2015; Sun et al. 2016; Ogawa et al. 2018; He et al. 2020). The negative interannual correlation between winter sea ice over the BKS and cold winters in CEU arises primarily because both are driven by the same anticyclonic circulation anomalies over the Ural region (Blackport et al. 2019). The Ural blocking (UB) is essential in inducing the WACE pattern, given that the BKS and CEU are influenced by warm and cold advection, respectively (Tyrlis et al. 2020). He et al. (2020) suggested that increased moisture and energy advection from the North Atlantic are necessary features when the WACE pattern is generated.

Previous studies based on observation data and model experiments have reported diverse results about the role of sea ice loss and internal atmospheric variability in the formation of the WACE pattern. The diversity is mainly attributable to the large internal atmospheric variability in the mid-latitudes and the difficulties in separating cause from effect (Screen et al. 2014; Blackport and Screen 2021). To address this issue, a large-ensemble simulation of an atmospheric general circulation model (AGCM) with perturbed initial conditions is useful, since it presents possible internal atmospheric variability realized under the identical lower boundary condition. This benefit helps distinguish the role of internal atmospheric variability in forming the WACE pattern. Therefore, the first objective of this study is to investigate the role of internal atmospheric variability in the observed interannual variation of the WACE pattern using a large-ensemble historical experiment.

Although some studies have already pointed out that several internal atmospheric variability processes are essential for the formation of the WACE pattern (e.g., Luo et al. 2016b; Blackport et al. 2019), their combined effect leading to the WACE pattern has not been quantitatively studied yet, owing to the limited sample size in observation. Hence, the second objective of this study is to quantitatively analyze the combined effect of internal atmospheric variability on the WACE pattern. The findings of this study are expected to improve the skill in predicting extreme cold weather over Eurasia by developing a deeper understanding of the linkage between the Arctic and the mid-latitude climate.

2 Data and methods

2.1 Data

The monthly temperature, sea-level pressure (SLP), wind, surface heat flux, and 6-hourly geopotential height data used in this study were obtained from the European Centre for Medium-Range Weather Forecasts Reanalysis v5 with horizontal resolution of 0.25°×0.25° (Hersbach et al. 2020). The observed monthly sea surface temperature (SST) and sea ice concentration (SIC) data were obtained from Centennial in situ Observation-Based Estimates of SST version 2 (COBE-SST2) with horizontal resolution of 1°×1° (Hirahara et al. 2014). For convenience, the reanalysis data are regarded as observation data in the remaining discussion.

This study used data from the "Database for Policy Decision-Making for Future Climate Change," produced by the Meteorological Research Institute AGCM version 3.2 with a high-resolution grid interval of 60 km (Mizuta et al. 2017). The large-ensemble size and the long-term simulation of this dataset provide the opportunity to analyze internal atmospheric variability. We adopted a historical experiment (hereafter, HIST) spanning 1951–2020, which was conducted by prescribing the observed SST and SIC from COBE-SST2 as the lower boundary conditions, and the observed greenhouse gases, aerosols, and ozone as external forcing (Mizuta et al. 2017; Imada et al. 2020). To analyze HIST for the period with reliable observation data, we focused our study on 1979–2020. HIST contains 100 members with perturbed initial conditions and boundary conditions. Therefore, the ensemble-mean can be considered as the response to the external forcing. In contrast, the variation among the ensemble members can be taken as a reflection of the internal atmospheric variability of the climate system

(i.e., the land–atmosphere system excluding the ocean component).

2.2 Method

We applied empirical orthogonal function (EOF) analysis separately to the observed and simulated winter (December–February) latitude-weighted SAT anomalies over Eurasia (20°–90° N, 0°–180° E) during 1979/1980–2019/2020 to extract the WACE pattern and its index. Overall, 4100 snapshots concatenated by 100 members over 41 years of simulated winter SAT anomalies were analyzed. Then, their corresponding principal components (PC) were rearranged on the time axis to present the PC for each member. The first leading mode denotes the continental warming pattern with positive SAT anomalies over the Eurasian continent (Additional file 1: Fig. S1a and S1c). The second leading mode denotes the WACE pattern with positive and negative SAT anomalies over the BKS and CEU, respectively (Additional file 1: Fig. S1b and S1d). The simulated WACE pattern is similar to that observed, with a spatial correlation coefficient of approximately 0.86 (Additional file 1: Fig. S1b and S1d). The time series of the observed and simulated second leading mode are defined as the observed WACE index and simulated WACE index for each member, respectively (Additional file 1: Fig. S1f and S1h).

Similarly, we also applied EOF analysis separately to the observed and simulated winter latitude-weighted SLP anomalies over the Atlantic sector (20°–80° N, 90° W–40° E) during 1979/1980–2019/2020 to determine the winter NAO pattern and its index. The first leading mode is defined as the winter NAO pattern, exhibiting opposite SLP anomalies over the Azores and Iceland (Additional file 2: Fig. S2a). The simulated winter NAO pattern is very similar to the observed winter NAO pattern, with a spatial correlation coefficient of 0.98 (not shown). The time series of the observed and simulated first leading modes are defined as the observed winter NAO index and simulated winter NAO index for each member, respectively (Additional file 2: Fig. S2b).

We calculated the UB frequency following Tibaldi and Molteni (1990), which considers the meridional gradient of daily 500-hPa geopotential height over 40°–80° E corresponding to the Ural region. Firstly, we calculated the daily northern meridional gradient $(Z_{80^\circ N+\Delta} - Z_{60^\circ N+\Delta})/((80^\circ N + \Delta) - (60^\circ N + \Delta))$ and daily southern meridional gradient $(Z_{60^\circ N+\Delta} - Z_{40^\circ N+\Delta})/((60^\circ N + \Delta) - (40^\circ N + \Delta))$ for each longitude. Here, Z is the 500-hPa geopotential height and Δ varies from $-5°$, 0°, to 5°. Secondly, blocking was detected on daily basis if the northern meridional gradient < -10 gpm per degree latitude and the southern meridional gradients > 0 for at least one of the Δ, and such condition persists for at least three consecutive days. Finally, after the detection of the blocking days, winter UB frequency was defined as the total blocking days averaged over 40°–80°E in each winter (Additional file 2: Fig. S2c). For observation and each member of the ensemble simulation, the standardized winter UB frequency for 41 years is used as the winter UB index.

3 Results

3.1 Observed and simulated winter temperature change over the Barents–Kara seas and Central Eurasia

The observed and simulated winter SAT and circulation trends are shown in Fig. 1a and b, respectively. There is an observed warming trend centered over the BKS and a cooling trend over CEU, with positive surface pressure and anticyclonic circulation trend over the Ural region (Fig. 1a). The ensemble-mean of the simulated winter SAT trend shows a similar but weaker warming trend over the BKS (Fig. 1b). Because the ensemble-mean trend could be considered as the trend due to external forcing, results above suggest the external forcing largely causes observed warming trend over the BKS. The positive surface pressure and anticyclonic circulation trend over the Ural region, and the cooling trend over CEU are not seen in the ensemble-mean fields (Fig. 1b). This implies that the influence of internal atmospheric variability is large in the observed cooling trend over CEU.

The interannual variation in winter SAT over the BKS and CEU is shown in Fig. 1c and d, respectively. Both the observed and the ensemble-mean of the simulated winter SAT over the BKS show a rapid increase, especially after the late 1990s (Fig. 1c) when the winter sea ice in this region started to decline rapidly, indicating a strong effect of local sea ice loss on SAT (Kim et al. 2019). Nevertheless, the intermember spread of the simulated winter SAT trend over the BKS is not negligible, as shown in Fig. 2, indicating that the effect of internal atmospheric variability could also perturb the observed winter warming over the BKS. In contrast to the rapid warming over the BKS, several observed cold winters occurred in CEU around 2010 (Fig. 1d). The intermember spread of the simulated winter SAT trend over CEU is very large, suggesting a crucial role of internal atmospheric variability on observed winter cooling over CEU (Fig. 2).

3.2 Second leading mode of winter temperature over Eurasia

The observed winter SAT trend in recent decades shows a WACE-like pattern (Figs. 1a and Additional file 1: S1b). EOF analysis was applied separately to the observed and simulated winter SAT anomalies over Eurasia to study the interannual variation of the WACE pattern. The second leading mode of the simulated winter SAT over

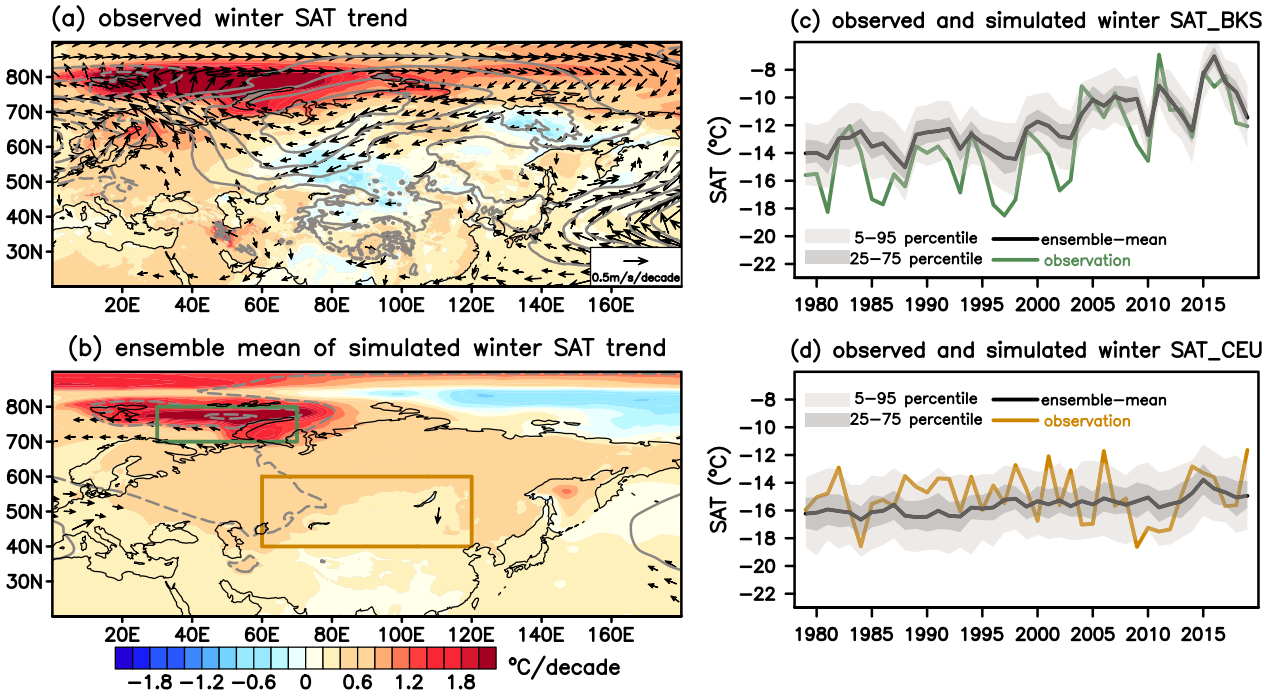

Fig. 1 Observed and simulated winter temperature change over the BKS and CEU. **a**, **b** Linear trends of winter SAT (shading; °C/decade), SLP (contour; hPa/decade; 0.2 intervals with negative values shown by dashed lines), and 850-hPa wind (vector; m/s/decade) for observations (**a**) and 100-member ensemble mean (**b**) during 1979/1980–2019/2020. Areas indicated by the green and orange lines in (**b**) denote the locations of the BKS (70°–80° N, 30°–70° E) and CEU (40°–60° N, 60°–120° E), respectively. **c**, **d** Interannual variation of observed and simulated winter SAT over the BKS and CEU, respectively, during 1979/1980–2019/2020. Green and orange lines denote observed winter SAT over the BKS and CEU, respectively; black lines denote the 100-member ensemble-mean; 25th–75th percentiles and 5th–95th percentiles of the ensemble spread are indicated by dark and light shading, respectively

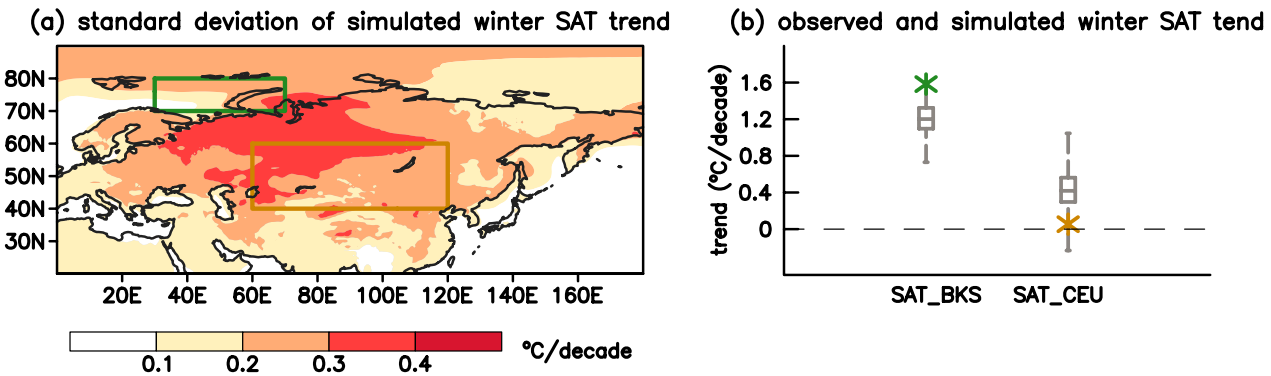

Fig. 2 Intermember spread of the simulated winter SAT trend. **a** The standard deviation of the 100-member simulated winter SAT trend (°C/decade). The green and orange regions denote the location of the BKS and CEU, respectively. **b** Observed (star) and simulated (box and whisker) winter SAT trends over the BKS and CEU. The upper and lower whiskers of the box are the maximum and minimum values, respectively; the upper and lower sides of the box are the upper and lower quartiles, respectively. Horizontal solid lines across the boxes denote the 100-member ensemble-mean

Eurasia exhibits a WACE structure, accounting for 14% of the total variance (Fig. 3a). The pattern shows a warm anomaly centered over the BKS and a cold anomaly centered over CEU, with an intensified surface high and an anticyclonic circulation over the Ural region (Fig. 3a). Both the observed and the ensemble-mean of the simulated WACE index increase rapidly after the late 1990s, suggesting a strong effect of the external forcing on the

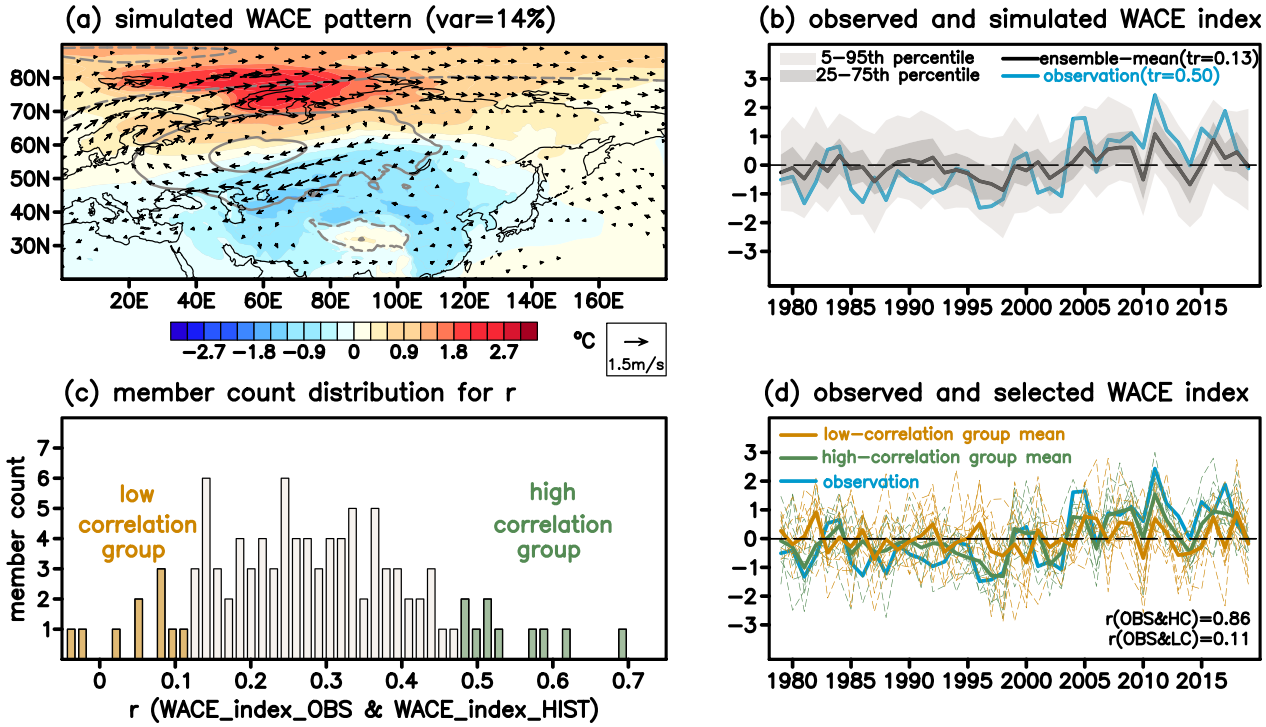

Fig. 3 Simulated WACE pattern and member selection. **a** Regression patterns of winter SAT (shading; °C), SLP (contour; hPa; 0.2 intervals with negative values shown by dashed lines), and 850-hPa wind (vector; m/s) anomalies against the member-concatenated simulated WACE index during 1979/1980–2019/2020. The specified value denotes the explained variance ratio. **b** Interannual variation of observed and simulated WACE index. Blue and black lines denote the observed WACE index and WACE index for the 100-member ensemble mean, respectively; 25th–75th percentiles and 5th–95th percentiles of the ensemble spread are indicated by dark and light shading, respectively. Numbers in parentheses denote the WACE index trend (σ/decade) during the study period. **c** Histogram of the interannual correlation coefficient between the observed WACE index and simulated WACE index for each member. Green and orange bars denote the 10 members of the high-correlation (HC) group and the 10 members of the low-correlation (LC) group, respectively. **d** Interannual variation of WACE index for the observation, high-correlation group, and low-correlation group. The blue line denotes the observed WACE index; thin and thick green lines denote the 10 members of the high-correlation group and their average, respectively; thin and thick orange lines denote the 10 members of the low-correlation group and their average, respectively

observed WACE index (Fig. 3b). Simultaneously, the simulated WACE index shows a large intermember spread, indicating that internal atmospheric variability also attributes to the observed interannual variation of the WACE pattern (Fig. 3b).

It is crucial to establish the extent to which internal atmospheric variability determines the observed interannual variation of the WACE pattern. To address this problem, two different groups of members extracted from the 100 members were selected, considering the similarity in the observed WACE index. Prior to this selection, the interannual correlation coefficient between the observed WACE index and simulated WACE index for each member was calculated, as summarized in Fig. 3c. We selected the 10 members with the highest correlation coefficient ($r > 0.47$) and the 10 members with the lowest correlation coefficient ($r < 0.11$); hereafter, they are referred to as the high-correlation group and the low-correlation group, respectively (Fig. 3c). The averaged winter SAT of the high-correlation group well reproduces the observed interannual variation of the winter SAT over the BKS ($r = 0.88$) and CEU ($r = 0.45$) (Additional file 3: Fig. S3). Hence, the averaged WACE index of the high-correlation group also shows high correlation against the observation ($r = 0.86$) (Fig. 3d). Conversely, the averaged winter SAT of the low-correlation group reproduces the observed interannual variation of winter SAT over the BKS ($r = 0.81$) (Additional file 3: Fig. S3a), mainly because of the prescribed SST and SIC, while it fails to reproduce the observed interannual variation of the winter SAT over CEU ($r = 0.05$) (Additional file 3: Fig. S3b). Hence, the averaged WACE index of the low-correlation group leads to low correlation against the observation ($r = 0.11$) (Fig. 3d). The diversity of simulated WACE index between the two groups is derived mainly from the difference in simulated winter SAT over CEU (Additional file 3: Fig. S3b). Because both groups are prescribed by the observed sea ice condition but have different

performances in simulating winter SAT over CEU and thus different WACE index, the two groups were compared to investigate the role of internal atmospheric variability in the mechanism of the observed cold winters in CEU and the formation of the WACE pattern.

3.3 Different circulation and temperature patterns related to winter sea ice decline over the Barents–Kara seas

The influence of sea ice decline over the BKS on the formation of cold winters in Eurasia has been proposed by many studies (e.g., Inoue et al. 2012; Mori et al. 2019). This subsection investigates different circulation and temperature patterns between the 10-member mean of the high-correlation group and the 10-member mean of the low-correlation group. Since the prescribed sea ice condition was identical in the high-correlation group and low-correlation group, the sea ice-induced atmospheric variability can be regarded as nearly the same between the two groups. The differences between the two groups are regarded as a manifestation of internal atmospheric variability.

Here, we study observed pressure and temperature patterns at the surface level related to winter sea ice decline. The regression analysis on sign-reversed SIC over the BKS shows higher surface pressure over the Ural region (Fig. 4a). It is also found that higher surface pressure over the Northern Atlantic and lower surface pressure over Iceland, indicating the presence of positive NAO. For the observed temperature pattern, there are positive and negative SAT anomalies over the BKS and CEU, respectively (Fig. 4a).

According to the similar regression analysis for the historical experiment, the high-correlation group shows a pattern similar to that of the observation, although the positive surface pressure anomaly over the Ural region and negative SAT anomaly over CEU are weaker in the high-correlation group (Fig. 4b). In contrast, the low-correlation group shows lower surface pressure over the Ural region, absence of positive NAO, and positive SAT anomaly over CEU (Fig. 4c).

The difference between the two groups, which is regarded as a manifestation of internal atmospheric variability, shows clear positive NAO phase and higher surface pressure over the Ural region, with positive and negative SAT anomalies over the BKS and CEU, respectively (Fig. 4d). This indicates the observed cold CEU is better reproduced when internal atmospheric variability resembles observation.

In the same way, the circulation and horizontal temperature advection pattern at the 850-hPa related to winter sea ice decline is investigated in Fig. 5. The circulation pattern at this level corresponds well with the surface pressure pattern (Figs. 4 and 5). The horizontal temperature advection pattern in the high-correlation group is similar to the observation, with a warm and cold advection over the BKS and CEU, respectively

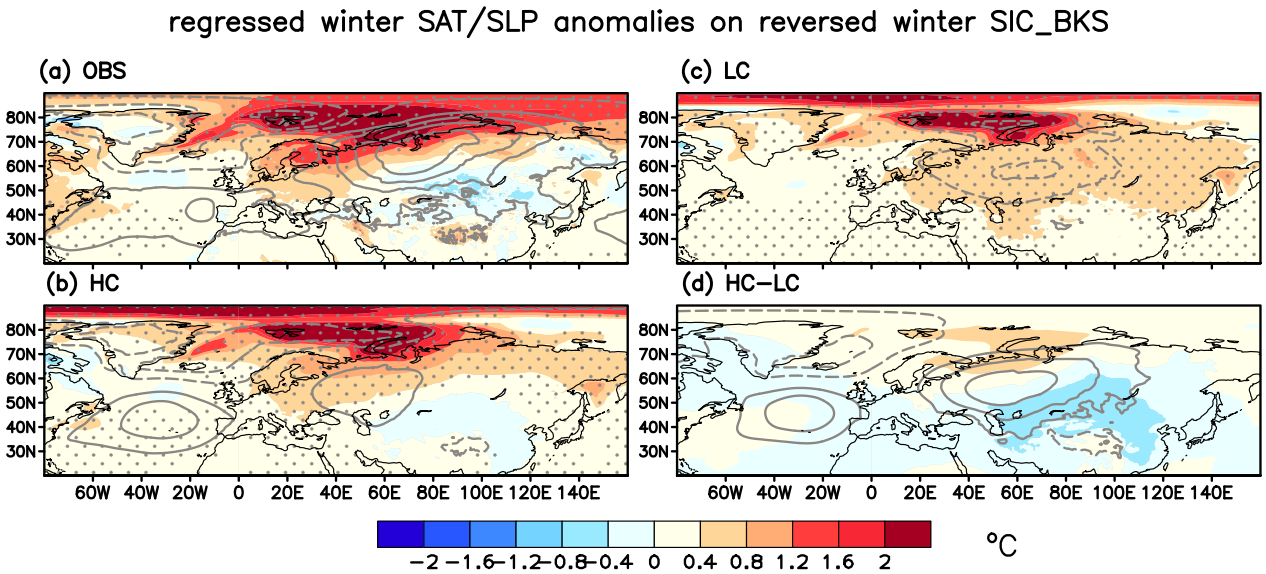

Fig. 4 Winter circulation and SAT patterns related to reversed winter sea ice change over the BKS. **a** Regressed observed winter SAT (shading; °C) and SLP (contour; hPa; 0.4 intervals with negative values shown by dashed lines) anomalies on observed winter SIC over the BKS. Note that SIC was sign-reversed and normalized. **b**, **c** Similar to (**a**), but (**b**) is for the 10-member mean of the high-correlation group, **c** is for the 10-member mean of the low-correlation group. **d** The difference between (**b**) and (**c**). Dots in **a**–**c** denote shading statistically significant at the 0.05 level by Student's t test

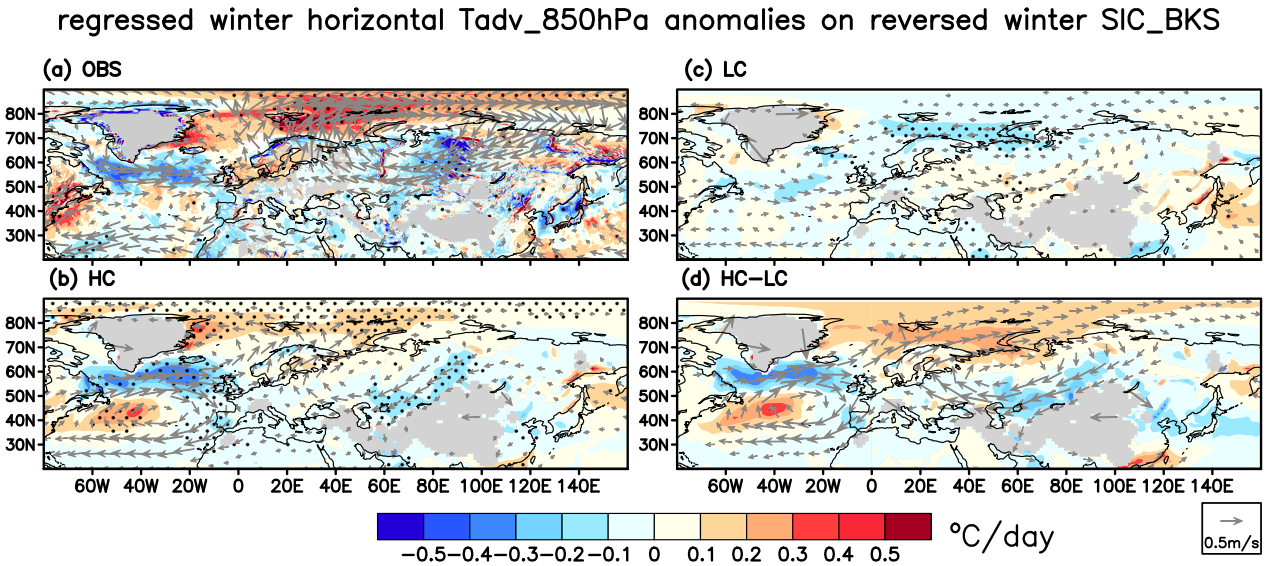

Fig. 5 Winter horizontal temperature advection pattern related to reversed winter sea ice change over the BKS. Similar to Fig. 4, but for winter horizontal temperature advection (shading; °C/day) and wind (vector; m/s) at 850-hPa. Dots in **a**–**c** denote shading statistically significant at the 0.05 level by Student's t test. The grey shadings in denote the topography

(Fig. 5a and b). On the contrary, the temperature advection pattern over the two regions is very weak or even reversed in the low-correlation group (Fig. 5c).

The difference between the high-correlation group and low-correlation group shows anticyclonic circulation anomalies over the Ural region and positive NAO (Fig. 5d). Their coincidence promotes warm advection, which is maintained mainly by meridional component, and increases the temperature over the BKS (Figs. 5d and Additional file 4: S4d). These features agree with Luo et al. (2017), which suggested this circulation pattern promotes the transport of moisture and heat from the North Atlantic near the Gulf Stream extension region, where SST is high, toward the BKS. Simultaneously, the northerly wind that dominates to the east of the Ural region enhances cold advection from the BKS to CEU, leading to a temperature decrease over CEU (Figs. 5d and Additional file 4: S4d). This result underscores the importance of internal atmospheric variability for forming the observed cold winters in CEU and the WACE pattern.

The southerly wind anomaly heading to BKS appears not to contribute to the sensible and latent heat flux over the BKS (Additional file 5: Fig. S5d and S5h). Actually, the warmer and wetter air from the Northern Atlantic tends to weaken sea-air temperature difference and humidity difference. As a result, it could mitigate turbulent heat flux from the ocean to the air.

3.4 Relationship between internal atmospheric variability and the WACE pattern

Figures 4 and 5 suggest that UB-like anticyclonic circulation and the NAO have essential impacts on the formation of the WACE pattern. This subsection quantitatively investigates the relationships among UB, the NAO, and the WACE pattern. The relationships are summarized in Fig. 6 based on the simulated 4100 years. The WACE index tends to be higher when both the UB index and NAO index are large (Fig. 6b). This result indicates that UB, together with the positive NAO, contributes substantially to the amplification of the WACE pattern, supporting the claim by Luo et al. (2016b).

The winter SAT over the BKS varies similarly to the WACE index in accordance with changes in winter UB and NAO (Fig. 6c), indicating that the WACE index largely reflects the variation of winter SAT over the BKS, as suggested by Komatsu et al. (2022). The winter SAT over the BKS tends to be warmer when both the UB index and NAO index are large (Fig. 6c). This is presumably because the circulation condition provides an efficient energy pathway from the North Atlantic to the BKS (Fig. 5; Luo et al. 2017). The quantitative analysis and regression analysis of the large simulation cases indicate similar contributions of the UB and positive NAO on the formation of warmer SAT over the BKS (Figs. 6c, Additional file 6: S6b and S6d).

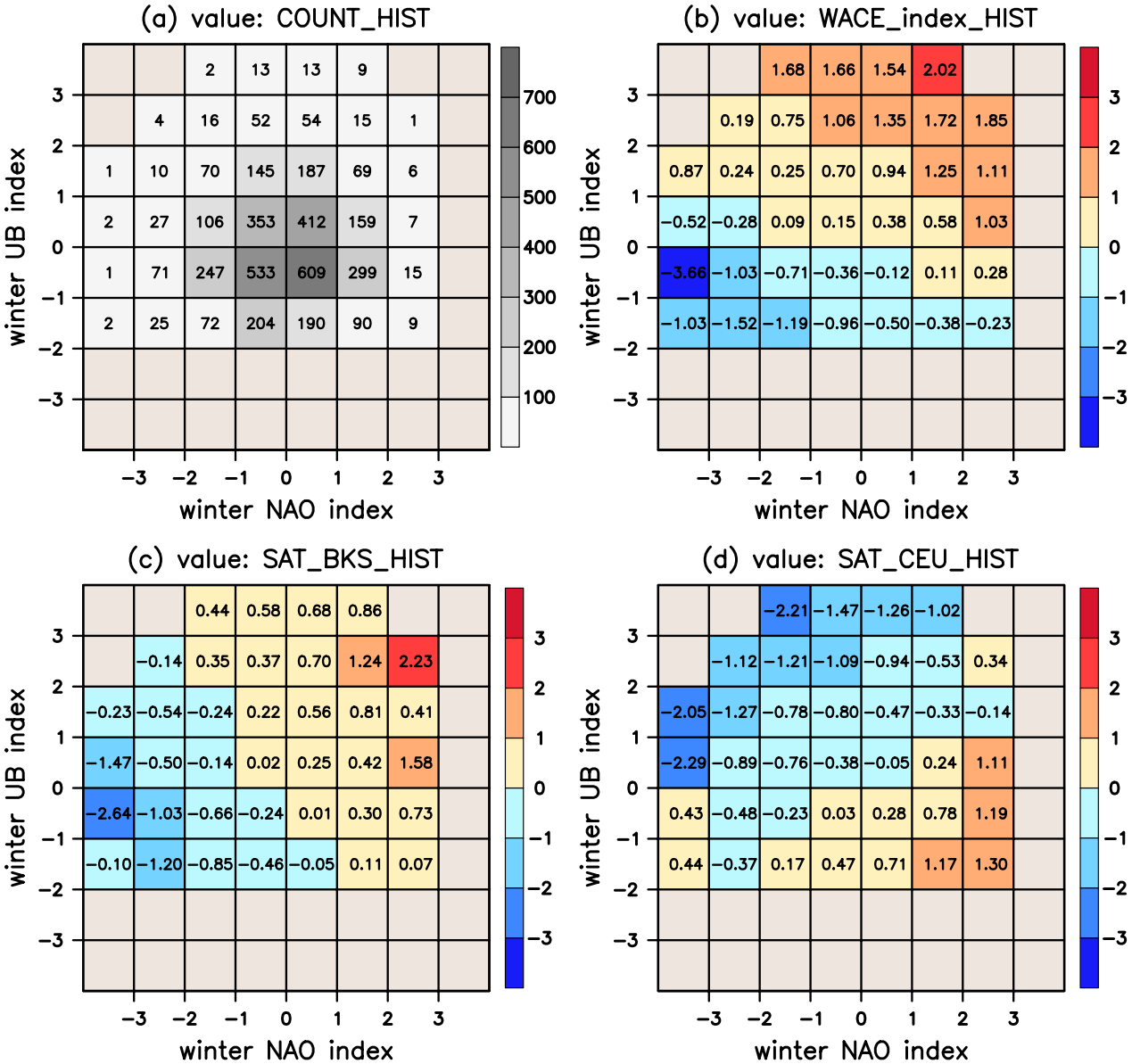

Fig. 6 Relationship between winter internal atmospheric variability and the WACE pattern for the simulated 4100 years. Scatterplot of the winter NAO and UB indexes. Values denote the year count (**a**), averaged WACE index (**b**), and standardized averaged winter SAT over the BKS (**c**) and CEU (**d**)

Winter SAT over CEU tends to be colder under the combination of UB and negative NAO (Fig. 6d). The effect of winter UB on cold CEU is more significant than negative NAO (Figs. 6d, Additional file 6: S6b, and S6d), probably because the negative NAO mainly decreases the temperature over northern Eurasia rather than CEU (Additional file 6: Fig. S6d). Although the observation results could reflect the relationships among UB, the NAO, and the WACE pattern, which are mainly similar to those large-ensemble show, the number of observed cases is limited to draw a robust conclusion (Additional file 6: Figs. S6a, S6c, and Additional file 7: S7).

4 Discussion

Some studies claimed the surface warming caused by sea ice loss over the BKS provides conditions favorable for the occurrence of UB (Luo et al. 2016a; Kim et al. 2022), which in turn amplifies local sea ice loss (Gong and Luo 2017; Tyrlis et al. 2020). Our study also investigated the relationship between winter SIC over the BKS and the

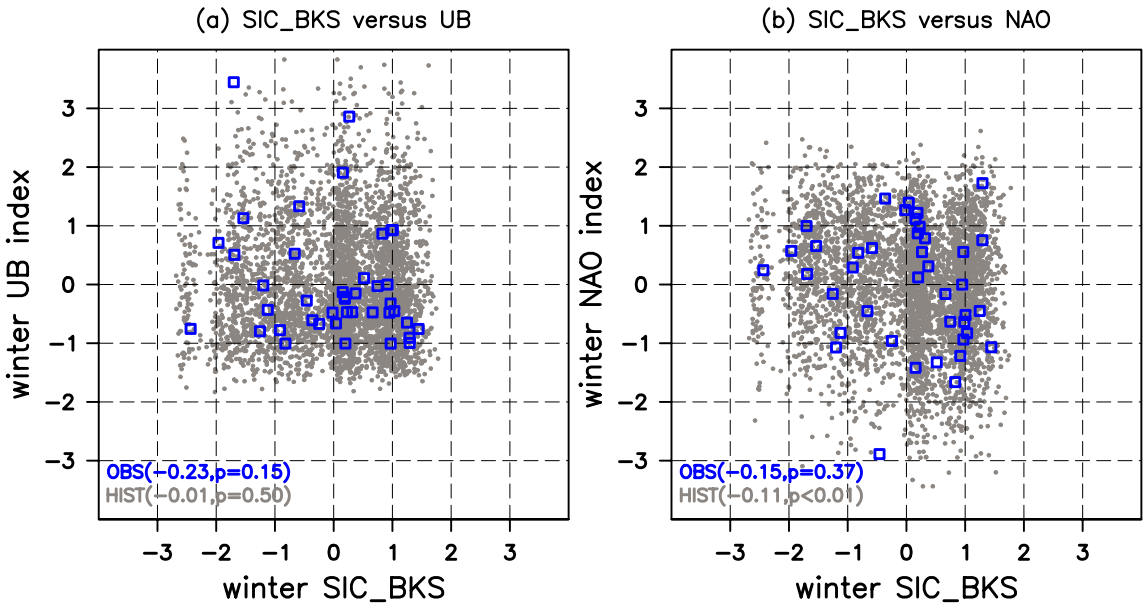

Fig. 7 Relationship between winter sea ice over the BKS and winter internal atmospheric variability. **a** Scatterplot for standardized winter SIC over the BKS and winter UB index for the observed 41 years (blue squares) and simulated 4100 years (grey dots). **b** Similar to **a**, but for the relationship between standardized winter SIC over the BKS and winter NAO index. The texts denote the correlation coefficient and p-value

winter UB frequency based on the large-ensemble historical experiment. Their correlation is not statistically significant in both observation and simulation (Fig. 7a), suggesting the influence of winter sea ice decline on winter UB frequency is weak. The robust two-way interaction between the sea ice loss and UB frequency at different timescales could be a future research topic. Early winter and late autumn sea ice loss tends to weaken the stratospheric polar vortex, leading to more frequent negative NAO state in winter (Kim et al. 2014; Nakamura et al. 2015). Results in this study suggest the negative correlation between winter sea ice over the BKS and winter NAO is very weak although positive NAO is slightly favored when sea ice declines (Fig. 7b).

Figure 8 presents the winter SAT and SLP anomalies related to winter sea ice decline over the BKS. The sea ice-induced atmospheric variability could be represented by the 100-member ensemble-mean, which establishes WACE-like temperature contrast between the BKS and CEU. In the high-correlation group, the internal atmospheric variability (Ural blocking and positive phase of NAO, Fig. 4b) possibly produces a warmer BKS and colder CEU than the ensemble-mean, leading to a greater WACE-like pattern (Fig. 8). On the other hand, in the low-correlation group, the internal atmospheric

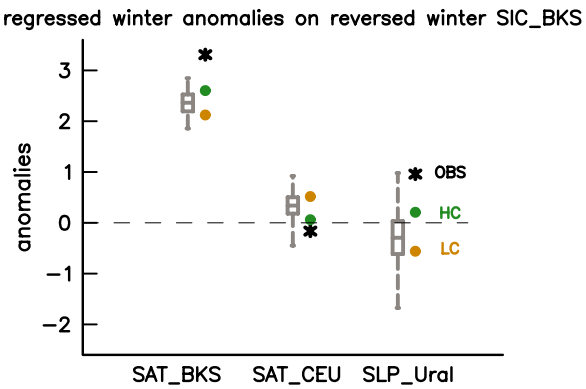

Fig. 8 Winter SAT and SLP anomalies related to winter sea ice decline over the BKS. Regressed winter SAT anomalies (°C) over the BKS (70°–80° N, 30°–70° E) and CEU (40°–60° N, 60°–120° E), and SLP anomalies (hPa) over the Ural region (40°–80° N, 40°–80° E) on reversed and normalized winter SIC over the BKS. The black stars and grey boxes denote the observation results and simulation results for each member, respectively. The upper and lower whiskers of the box are the maximum and minimum values, respectively; the upper and lower sides of the box are the upper and lower quartiles, respectively. Horizontal solid lines across the boxes denote the 100-member ensemble-mean. The green and orange dots denote the 10-member mean of the high-correlation group and 10-member mean of the low-correlation group, respectively

variability (negative SLP anomalies over the Ural region, Fig. 4c) acts oppositely to what happens in the high-correlation group. Hence, the atmospheric response to sea ice is obscured (Fig. 8). Overall, the internal atmospheric variability in the high-correlation group and low-correlation group both affects the WACE pattern, but their roles are opposite.

Finally, we will discuss the limitation of the current study. The large-ensemble historical simulation adopted in this study was created using the AGCM. As in Fig. 8, the model is likely to underestimate the SAT anomaly over the BKS related to local sea ice decline. Despite that, the observed SLP anomaly over the Ural region and SAT anomaly over CEU are within the range of the ensemble spread (Fig. 8). These results imply that the model has the ability to simulate SLP anomaly over the Ural region and SAT anomaly over CEU as they are observed. However, there is the possibility that the underestimated SAT anomalies over the BKS can indirectly cause underestimation of the cold CEU. Experiments with two-way atmosphere–ocean coupling configuration will be suitable for the investigation of sea ice impact. Large-ensemble experiment conducted by the atmosphere–ocean general circulation model is desired for further investigation of the WACE pattern.

5 Conclusion

This study analyzes a large-ensemble historical experiment to investigate the roles of internal atmospheric variability in the observed interannual variation of the WACE pattern. Analysis of the observed and simulated winter SAT change over the BKS indicates that the warming trend over the BKS is mainly caused by external forcing, but the contribution of internal atmospheric variability cannot be ignored (Figs. 1 and 2). On the contrary, the winter cooling trend over CEU is largely regulated by the internal atmospheric variability (Figs. 1 and 2).

Results of EOF analysis on winter SAT anomalies over Eurasia suggest that both external forcing and internal atmospheric variability contribute to the observed interannual variation of the WACE pattern (Fig. 3b). Comparison of ensemble members suggests UB-like anticyclonic circulation and the NAO are the key internal atmospheric variability responsible for the observed interannual variation of the WACE pattern (Fig. 4). The UB-like anticyclonic circulation, together with the positive NAO phase, provides an efficient energy transport pathway from the North Atlantic to the BKS, promoting warm advection and increasing regional winter SAT over the BKS (Fig. 5). The northerly wind that dominates to the east of the Ural region enhances cold advection and reduces regional winter SAT over CEU (Fig. 5).

This study also quantitatively analyzes the combined effect of UB and NAO on the WACE pattern using a large-ensemble experiment. Results indicate similar contributions of the UB and positive NAO on the formation of warmer SAT over the BKS (Fig. 6c). The effect of winter UB to form colder CEU is greater than that of the negative NAO (Fig. 6d).

Other factors, such as winter tropical Pacific cooling and autumn snow cover reduction, also contribute to cold winters in CEU (Matsumura and Kosaka 2019; Luo et al. 2021; Xu et al. 2018). Recent changes in the Arctic Ocean have altered the hydrological cycle in circumpolar terrestrial regions (Sato et al. 2022). Hence, it is necessary to study the variability in land–atmosphere interaction over CEU in the future. Hori and Oshima (2018) compared the WACE pattern using large-ensemble experiments under historical simulation and non-warming simulation. Considering the possible interaction between sea ice loss and internal atmospheric variability, future studies could utilize large-ensemble experiments to investigate the sensitivity of the future WACE pattern under continuing reduction of Arctic sea ice.

This study focuses on the seasonal mean SAT pattern. The follow-on studies are expected to conduct the analysis of daily to subseasonal timescale to understand the development of the WACE pattern as such aspect drew attention in recent studies (Tyrlis et al. 2020; Kim et al. 2021; Yin et al. 2023). The subseasonal analysis for the development of internal atmospheric variability and temperature anomalies over the key regions using large-ensemble experiments could be a future research topic.

Abbreviations

AGCM	Atmospheric general circulation model
BKS	Barents–Kara seas
CEU	Central Eurasia
COBE	Centennial in situ Observation-Based Estimates
EOF	Empirical orthogonal function
HIST	Historical experiment
HC	High-correlation
LC	Low-correlation
NAO	North Atlantic Oscillation
PC	Principal component
SAT	Surface air temperature
SIC	Sea ice concentration
SLP	Sea-level pressure
SST	Sea surface temperature
UB	Ural blocking
WACE	Warm Arctic–Cold Eurasia

Supplementary Information

The online version contains supplementary material available at https://doi.org/10.1186/s40645-023-00591-x.

Additional file 1. Figure S1. Two leading modes governing the winter temperature over Eurasia.

Additional file 2. Figure S2. Winter NAO index and UB frequency.

Additional file 3. Figure S3. Winter temperature change over the BKS and CEU in selected two groups.

Additional file 4. Figure S4. Winter meridional and zonal temperature advection pattern related to reversed winter sea ice change over the BKS.

Additional file 5. Figure S5. Winter sensible and latent heat flux pattern related to reversed winter sea ice change over the BKS.

Additional file 6. Figure S6. Winter SAT pattern related to internal atmospheric variability change.

Additional file 7. Figure S7. Relationships among winter UB, the NAO, and the WACE pattern for the observed 41 years.

Acknowledgements
We thank James Buxton MSc, from Edanz (https://jp.edanz.com/ac), for editing a draft of this manuscript. We also appreciate the editor and two anonymous reviewers for their constructive comments.

Author contributions
XZ proposed the topic, analyzed the data, and wrote the original manuscript. TS and LS advised the analysis and helped in the interpretation of the results and the revision of the manuscript.

Funding
This study was supported by the Japan Society for the Promotion of Science KAKENHI (Grant Number: JP19H05668), the Arctic Challenge for Sustainability II (ArCSII) project (Grant Number: JPMXD1420318865), the SENTAN program (JPMXD0722680734), and the JST SPRING (Grant Number: JPMJSP2119), Japan.

Availability of data and materials
The atmosphere data from European Centre for Medium-Range Weather Forecasts Reanalysis v5 are available at https://cds.climate.copernicus.eu/cdsapp#!/search?type=dataset. The SST and SIC data from Centennial Observation-Based Estimates of SST Version 2 are available at https://psl.noaa.gov/data/gridded/data.cobe2.html. The historical simulation data from Database for Policy Decision-Making for Future Climate Change are available at http://d4pdf.diasjp.net/d4PDF.cgi.

Declarations

Competing interests
The authors declare that they have no competing interest.

Received: 28 April 2023 Accepted: 16 September 2023
Published online: 03 October 2023

References

Blackport R, Screen JA, van der Wiel K, Bintanja R (2019) Minimal influence of reduced Arctic sea ice on coincident cold winters in mid-latitudes. Nat Clim Change 9:697–704. https://doi.org/10.1038/s41558-019-0551-4

Blackport R, Screen JA (2021) Observed statistical connections overestimate the causal effects of Arctic sea ice changes on midlatitude winter climate. J Clim 34:3021–3038. https://doi.org/10.1175/JCLI-D-20-0293.1

Cohen J, Screen JA, Furtado JC, Barlow M, Whittleston D, Coumou D, Francis J, Klaus D, Entekhabi D, Overland J, Jones J (2014) Recent Arctic amplification and extreme mid-latitude weather. Nat Geosci 7:627–637. https://doi.org/10.1038/ngeo2234

Gong T, Luo D (2017) Ural Blocking as an amplifier of the Arctic sea ice decline in winter. J Clim 30:2639–2654. https://doi.org/10.1175/JCLI-D-16-0548.1

Hersbach H, Bell B, Berrisford P, Hirahara S, Horányi A, Muñoz-Sabater J, Nicolas J, Peubey C, Radu R, Schepers D, Simmons A, Soci C, Abdalla S, Abellan X, Balsamo G, Bechtold P, Biavati G, Bidlot J, Bonavita M, Chiara GD, Dahlgren P, Dee D, Diamantakis M, Dragani R, Flemming J, Forbes R, Fuentes M, Geer A, Haimberger L, Healy S et al (2020) The ERA5 global reanalysis. Q J R Meteorol Soc 146:1999–2049. https://doi.org/10.1002/qj.3803

He S, Xu X, Furevik T, Gao Y (2020) Eurasian cooling linked to the vertical distribution of Arctic warming. Geophys Res Lett 47:e2020GL087212. https://doi.org/10.1029/2020GL087212

Hirahara S, Ishii M, Fukuda Y (2014) Centennial-scale sea surface temperature analysis and its uncertainty. J Clim 27:57–75. https://doi.org/10.1175/JCLI-D-12-00837.1

Hori ME, Oshima K (2018) Robustness of the warm arctic/cold Eurasian signature within a large ensemble model experiment. Sci Online Lett Atmos 14:69–73. https://doi.org/10.2151/sola.2018-012

Imada Y, Kawase H, Watanabe M, Arai M, Shiogama H, Takayabu I (2020) Advanced risk-based event attribution for heavy regional rainfall events. Npj Clim Atmos Sci 3:37. https://doi.org/10.1038/s41612-020-00141-y

Inoue J, Hori M, Takaya K (2012) The role of Barents sea ice in the wintertime cyclone track and emergence of a warm-Arctic cold Siberian anomaly. J Clim 25:2561–2568. https://doi.org/10.1175/JCLI-D-11-00449.1

Isaksen K, Nordli Ø, Ivanov B, Køltzow MAØ, Aaboe S, Gjelten HM, Mezghani A, Eastwood S, Førland E, Benestad RE, Hanssen-Bauer I, Brækkan R, Sviashchennikov P, Demin V, Revina A, Karandasheva T (2022) Exceptional warming over the Barents area. Sci Rep 12:9371. https://doi.org/10.1038/s41598-022-13568-5

Johnson NC, Xie SP, Kosaka Y, Li X (2018) Increasing occurrence of cold and warm extremes during the recent global warming slowdown. Nat Commun 9:1724. https://doi.org/10.1038/s41467-018-04040-y

Kim BM, Son SW, Min SK, Jeong JH, Kim SJ, Zhang X, Shim T, Yoon JH (2014) Weakening of the stratospheric polar vortex by Arctic sea-ice loss. Nat Commun 5:4646. https://doi.org/10.1038/ncomms5646

Kim HJ, Son SW, Moon W, Kug JS, Hwang J (2021) Subseasonal relationship between Arctic and Eurasian surface air temperature. Sci Rep 11:4081. https://doi.org/10.1038/s41598-021-83486-5

Kim KY, Kim JY, Kim J, Yeo S, Na H, Hamlington BD, Leben RR (2019) Vertical feedback mechanism of winter Arctic amplification and sea ice loss. Sci Rep 9:1184. https://doi.org/10.1038/s41598-018-38109-x

Kim SH, Sung HJ, Kim SJ, Baek EH, Moon JY, Kim BM (2022) Contribution of Ural and Kamchatka Blockings to the amplified Warm Arctic-Cold Eurasia pattern under Arctic sea ice loss and Eurasian cooling. J Clim 35:4071–4083. https://doi.org/10.1175/JCLI-D-21-0635.1

Komatsu K, Takaya Y, Toyoda T, Hasumi H (2022) Response of Eurasian Temperature to Barents-Kara Sea Ice: Evaluation by Multi -Model Seasonal Predictions. Geophys Res Lett 49:e2021GL097203. https://doi.org/10.1029/2021GL097203

Li C, Stevens B, Marotzke J (2015) Eurasian winter cooling in the warming hiatus of 1998–2012. Geophys Res Lett 42:8131–8139. https://doi.org/10.1002/2015GL065327

Luo B, Luo D, Dai A, Simmonds I, Li Wu (2021) A connection of winter Eurasian cold anomaly to the modulation of Ural Blocking by ENSO. Geophys Res Lett 48:e2021GL094304. https://doi.org/10.1029/2021GL094304

Luo B, Luo D, Wu L, Zhong L, Simmonds I (2017) Atmospheric circulation patterns which promote winter Arctic sea ice decline. Environ Res Lett 12:054017. https://doi.org/10.1088/1748-9326/aa69d0

Luo D, Xiao Y, Yao Y, Dai A, Simmonds I, Franzke C (2016a) Impact of Ural Blocking on winter Warm Arctic-Cold Eurasian anomalies Part i: Blocking-Induced Amplification. J Clim 29:3925–3947. https://doi.org/10.1175/JCLI-D-15-0611.1

Luo D, Xiao Y, Diao Y, Dai A, Franzke C, Simmonds I (2016b) Impact of ural blocking on winter Warm Arctic–Cold Eurasian anomalies. Part II: The link to the North Atlantic Oscillation. J Clim 29:3949–3971. https://doi.org/10.1175/JCLI-D-15-0612.1

Matsumura S, Kosaka Y (2019) Arctic-Eurasian climate linkage induced by tropical ocean variability. Nat Commun 10:3441. https://doi.org/10.1038/s41467-019-11359-7

McCusker K, Fyfe J, Sigmond M (2016) Twenty-five winters of unexpected Eurasian cooling unlikely due to Arctic sea-ice loss. Nat Geosci 9:838–842. https://doi.org/10.1038/ngeo2820

Mizuta R, Murata A, Ishii M, Shiogama H, Hibino K, Mori N, Arakawa O, Imada Y, Yoshida K, Aoyagi T, Kawase H, Mori M, Okada Y, Shimura T, Nagatomo T, Ikeda M, Endo H, Nosaka M, Arai M, Takahashi C, Tanaka K, Takemi T, Tachikawa Y, Temur K, Kamae Y, Watanabe M, Sasaki H, Kitoh A, Takayabu I, Nakakita E, Kimoto M (2017) Over 5000 years of ensemble future climate simulations by 60-km Global and 20-km Regional Atmospheric Models. Bull Am Meteorol Soc 98:1383–1398. https://doi.org/10.1175/BAMS-D-16-0099.1

Mori M, Kosaka Y, Watanabe M, Nakamura H, Kimoto M (2019) A reconciled estimate of the influence of Arctic sea-ice loss on recent Eurasian cooling. Nat Clim Change 9:123–129. https://doi.org/10.1038/s41558-018-0379-3
Mori M, Watanabe M, Shiogama H, Inoue J, Kimoto M (2014) Robust Arctic sea-ice influence on the frequent Eurasian cold winters in past decades. Nat Geosci 7:869–873. https://doi.org/10.1038/ngeo2277
Nakamura T, Yamazaki K, Iwamoto K, Honda M, Miyoshi Y, Ogawa Y, Ukita J (2015) A negative phase shift of the winter AO/ NAO due to the recent Arctic sea-ice reduction in late autumn. J Geophys Res Atmos 120:3209–3227. https://doi.org/10.1002/2014JD022848
Ogawa F, Keenlyside N, Gao Y, Koenigk T, Yang S, Suo L, Wang T, Gastineau G, Nakamura T, Cheung HM, Omani NE, Ukita J, Semenov V (2018) Evaluating impacts of recent Arctic sea ice loss on the Northern Hemisphere winter climate change. Geophys Res Lett 45:3255–3263. https://doi.org/10.1002/2017GL076502
Rantanen M, Karpechko AY, Lipponen A, Nordling K, Hyvärinen O, Ruosteenoja K, Vihma T, Laaksonen A (2022) The Arctic has warmed nearly four times faster than the globe since 1979. Commun Earth Environ 3:168. https://doi.org/10.1038/s43247-022-00498-3
Sato T, Nakamura T, Iijima Y, Hiyama T (2022) Enhanced Arctic moisture transport toward Siberia in autumn revealed by tagged moisture transport model experiment. Npj Clim Atmos Sci 5:91. https://doi.org/10.1038/s41612-022-00310-1
Stroeve J, Notz D (2018) Changing state of Arctic sea ice across all seasons. Environ Res Lett 13:103001. https://doi.org/10.1088/1748-9326/aade56
Screen JA, Deser C, Simmonds I, Tomas R (2014) Atmospheric impacts of Arctic sea-ice loss, 1979–2009: separating forced change from atmospheric internal variability. Clim Dyn 43:333–344. https://doi.org/10.1007/s00382-013-1830-9
Sun L, Perlwitz J, Hoerling M (2016) What caused the recent "Warm Arctic, Cold Continents" trend pattern in winter temperatures? Geophys Res Lett 43:5345–5352. https://doi.org/10.1002/2016GL069024
Tyrlis E, Bader J, Manzini E, Ukita J, Nakamura H, Matei D (2020) On the role of Ural Blocking in driving the Warm Arcit-Cold Siberia Pattern. Q J R Meteorol Soc 146:2138–2153. https://doi.org/10.1002/qj.3784
Tibaldi S, Molteni F (1990) On the operational predictability of blocking. Tellus A Dyn Meteorol Oceanogr. https://doi.org/10.3402/tellusa.v42i3.11882
Wang S, Chen W (2022) Impact of internal variability on recent opposite trends in wintertime temperature over the Barents-Kara Seas and central Eurasia. Clim Dyn 58:2941–2956. https://doi.org/10.1007/s00382-021-06077-0
Xu X, He S, Li F, Wang H (2018) Impact of northern Eurasian snow cover in autumn on the warm Arctic-cold Eurasia pattern during the following January and its linkage to stationary planetary waves. Clim Dyn 50:1993–2006. https://doi.org/10.1007/s00382-017-3732-8
Yin Z, Zhang Y, Zhou B, Wang H (2023) Subseasonal variability and the "Arctic warming-Eurasia cooling" trend. Sci Bull. https://doi.org/10.1016/j.scib.2023.02.009
Zhang P, Wu Y, Simpson I, Smith K, Zhang X, De B, Callaghan P (2018) A stratospheric pathway linking a colder Siberia to Barents–Kara Sea sea ice loss. Sci Adv 4(7):eaat6025. https://doi.org/10.1126/sciadv.aat6025

Publisher's Note